Steady-State and Transient Electrothermal Simulation of Microheater for Gas Sensing

A. N. Radwan and Mehran Mehregany
Department of Electrical Engineering and Computer Science, Case Western Reserve University, Cleveland, OH, USA
anr43@case.edu, mehran@case.edu

Abstract:
We report steady-state and transient electrothermal analyses of a microheater to study the time required for it to reach an intended operating temperature—normally 400 °C to 600 °C. Our gas sensor model is comprised of a glass substrate, covered with a silicon dioxide (SiO_2) layer upon which a patterned polysilicon (PolySi) heating resistor and a subsequent tin oxide (SnO_2) sensing layer are formed. For a 2.5V and 1.4V bias of the microheater, steady-state temperatures of ~900 °C and 400 °C were reached, respectively—both in 5 s.

Keywords: microheater, low power consumption, metal oxide, gas sensor, response time, glass substrate

1. Introduction

Metal oxide based gas sensors—using microelectromechanical systems (MEMS) technology—have been gaining momentum in recent years. They are comparatively simple to use, low in cost and capable of detecting a variety of gases. A sensing material (typically tin oxide, SnO_2) is situated on top of a patterned heating resistor—usually referred to as a microheater. The role of the microheater is to heat the sensing material to an operating temperature that enhances its sensitivity and selectivity, thereby improving the gas sensing performance. SnO_2 for example can detect a variety of harmful gases such as CO, CH_4, NO_2 and C_3H_8 through its change in electrical conductivity [12, 13].

The electrothermal properties of resistive microheaters used for gas sensing applications have been studied analytically and experimentally. Previously reported studies in COMSOL™ proceedings have shed light on microheaters' thermal properties, optimized geometries and power consumptions—all based on steady-state electrothermal analysis. However, a critical gas sensor performance parameter—not studied—is response time, defined *as the time required for the sensor to respond to the minimum detectable gas concentration value*.

In this paper, we report on the steady-state and transient electrothermal performance of a resistive microheater using COMSOL™. Figure 1 shows a three-dimensional (3D) schematic of our gas sensor chip. The materials incorporated in the *Model Builder* are silica glass, SiO_2, polysilicon (PolySi), Platinum (Pt) and SnO_2. Their respective thicknesses are 300 µm, 3 µm, 2 µm, 2 µm and 0.2 µm.

In the following sections, we present the COMSOL™ mathematical modeling, model setup, steady-state and transient thermal analysis.

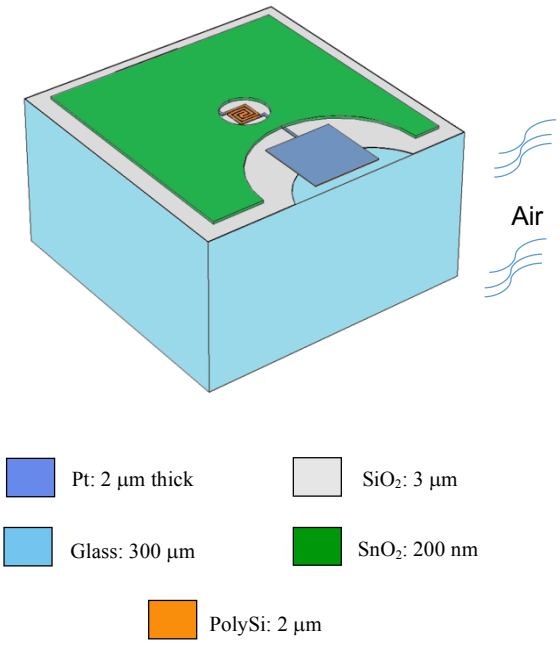

Figure 1. A 3D schematic of our gas sensor chip. (The graphical semicircle sectioning is to show the underlying layers and is not part of the actual design.)

2. Mathematical Modeling

The mathematical modeling used in COMSOL™ within the *Heat Transfer in Solids* module is the heat equation, given by:

$$\rho C_p \frac{dT}{dt} - \Delta(k \Delta T) = Q \qquad (1)$$

where C_p is the heat capacity, ρ is the material density, $\frac{dT}{dt}$ is the rate of temperature change per unit time t, k is the thermal conductivity, and Q is the heat source.

Joule heating, or Ohmic heating, is a process by which the body temperature increases due to resistive heating as a result of an applied electric current. The heating term Q is given by:

$$Q = J E = J\left(\frac{J}{\sigma}\right) = \frac{1}{\sigma} J^2 = \rho J^2 \qquad (2)$$

where E is the electric field, and J is the current density. It is seen in Equation (2) that the resistive heat Q is proportional to the square of the magnitude of the electric density J. Also, the electric resistivity ρ is a function of temperature:

$$\rho(T) = \rho_o\left[1 + \alpha\left(T - T_o\right)\right] \qquad (3)$$

where α is the temperature coefficient of resistivity. T_o and ρ_o are referred to in COMSOL™ as the reference temperature and resistivity, respectively. In our work, we set the reference temperature equal to the room temperature (293 K).

The electric power consumption is given by:

$$P = I^2 R \qquad (4)$$

where I is the applied electric current, and R is the microheater's resistance value.

3. Model Setup

a) Heater Design

Figure 2 shows a schematic of the resistive microheater model. The inset in Figure 2 shows the PolySi spiral microheater. The spiral traces are 5.0 µm wide and the spiral gaps are 2.5 µm wide. The microheater was designed to provide efficient heat confinement. The square Pt contact pads are 150 µm on each side and reach the PolySi spiral microheater with 5 µm-wide, 105 µm-long Pt traces.

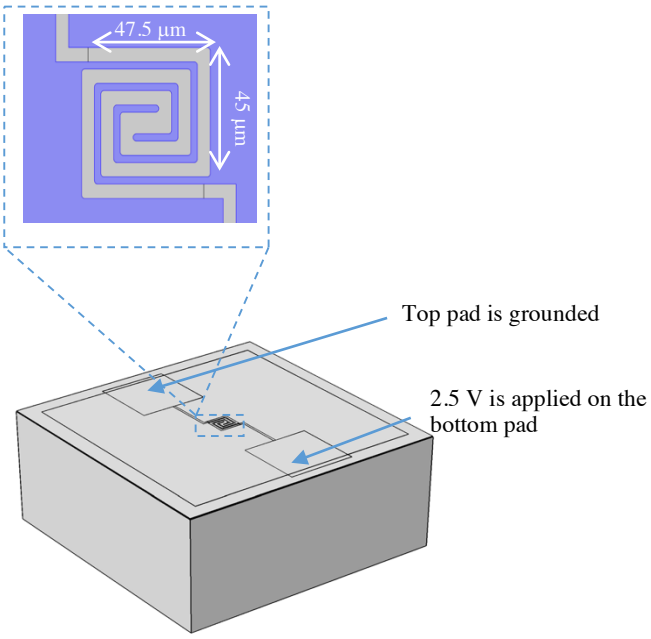

Figure 2. The 3D microheater model, with the inset a close-up view of the spiral heater.

b) Material Properties

Table 1 lists the material properties input in the model builder.

c) Electrothermal Setup

The *Electric Current* (*ec*) module was used to apply a DC voltage to the microheater. We applied a 2.5V and 0V (i.e., ground) boundary *Electric Potential* on the contact pads as shown in Figure 2. We used the *Heat Transfer in Solids* (*ht*) interface to model heat transfer by conduction and convection simultaneously. The former used the COMSOL™ built-in defined heat equation (Equation 1) whereas the latter was based upon the following convective heat flux equation:

$$q_0 = h\left(T_{ext} - T\right) \qquad (5)$$

where h is the convective heat transfer coefficient—set to 30 W/(m^2 . K). In our model, the medium is air, i.e., h varies from 10 to 100 W/(m^2 . K). While the convective transfer coefficient is dependent upon the geometry and the fluid motion, it has a negligible effect on micro-devices. Comparisons of mathematical and empirical h results have been previously reported [16, 17].

Table 1: List of material properties defined in the model builder.

Property	Unit	Pt	PolySi*	Silica Glass*	SnO_2	SiO_2	Refs
Density (ρ)	Kg/m^3	21450	2320	2203	6990	2160	[1-3]
Thermal Conductivity (κ)	W/(m.K)	69.1	k(T)**	1.38	13	0.9	[3-5]
Heat capacity at constant pressure (C_p)	J/(kg.K)	133	678	703	293	722	[1, 6, 7]
Reference resistivity (ρ_o)	Ω.m	106×10^{-9}	2×10^{-5}	1×10^{15}	66×10^{-6}	1×10^{17}	[8-10]
Resistivity temperature coefficient (α)	K^{-1}	3.92×10^{-3}	1.25×10^{-3}	1×10^{-16}	2×10^{-5}	0.0***	[10, 11]
Relative permittivity (ε)	-	N/A	4.5	2.09	3.78	3.7	[12, 14, 15]

*A built-in defined COMSOL™ material. **Defined analytically by COMSOL™ as a function of T.
***No value has been reported in the literature, hence set to zero in the model.

d) Meshing

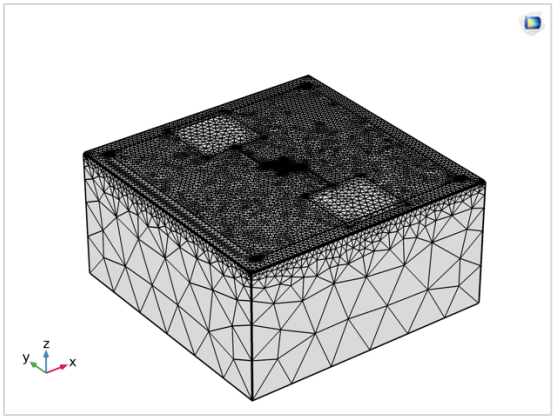

Figure 3. Meshed microheater model using the free tetrahedral operation.

Since our device has varying layer thicknesses, we applied the 3D free tetrahedral meshing option twice on two portions of the microheater (Figure 3). The first portion had thin films including the SnO_2, SiO_2 and the PolySi layer, while the second portion was the bulk glass substrate.

4. Results

a) Steady-State Response

Figure 4a shows the surface electric potential distribution related to the direct current flowing through the microheater. Figure 4b shows the resulting temperature distribution on the microheater. The temperature varies from 840 °C, around the central point, to a little over 900 °C near the PolySi-Pt junctions. (The potential difference is maximum at Pt-PolySi junctions.) In Figure 5a, we varied the microheater's bias voltage from 0V to 2.5V in order to observe the temperature-voltage curve. The temperature increased nonlinearly as the voltage increased.

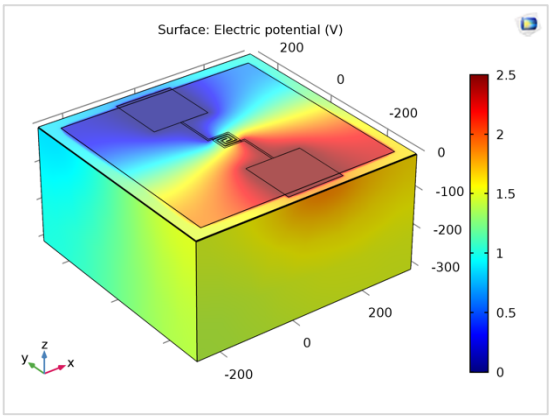

(a)

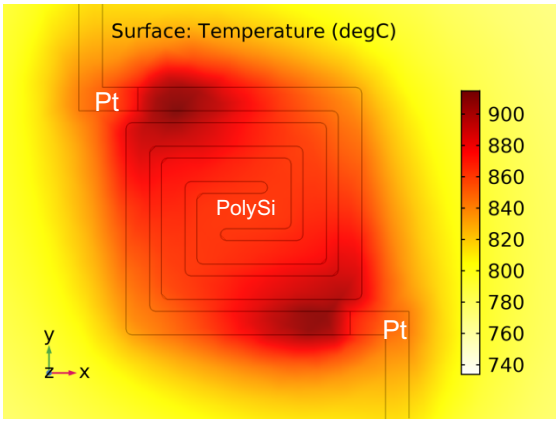

(b)

Figure 4. Microheater analysis: (a) surface electric potential distribution; and (b) surface temperature distribution.

Lastly, we generated the resistance-temperature curve (Figure 5b) for the microheater. At room temperature, the microheater resistance was nearly 60Ω. It increased linearly as the temperature increased, with a temperature coefficient of 0.0998.

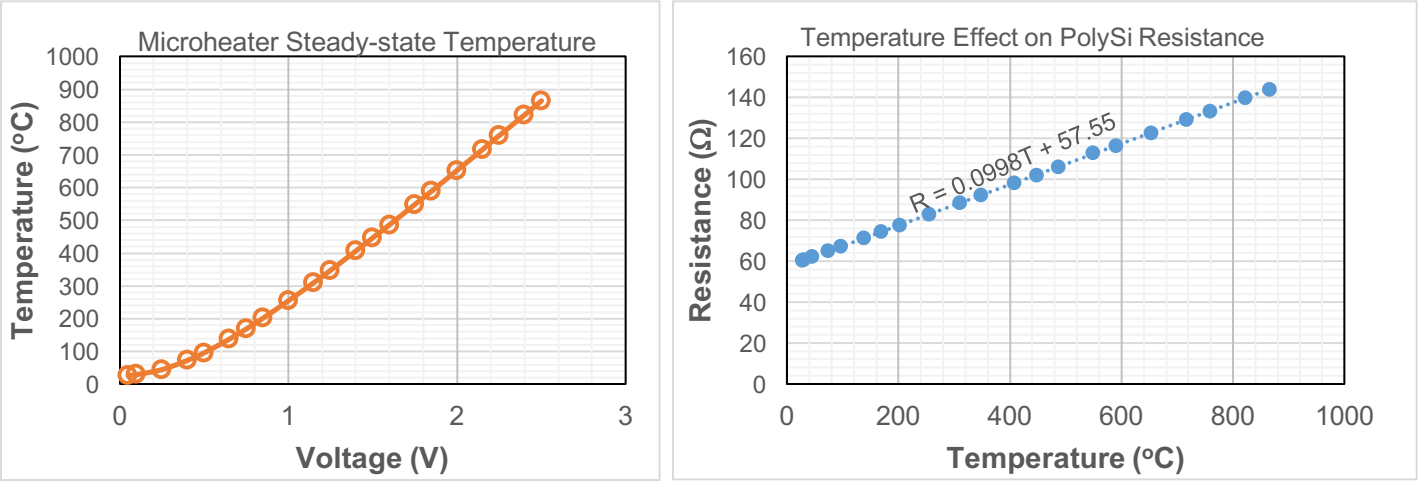

(a) (b)

Figure 5. Microheater analysis: (a) temperature versus applied bias; and (b) resistance versus temperature.

b) Transient Response

Since the sensing layer SnO_2 reacts with various gases at different operating temperatures, simulating the transient thermal response is the basis of determining the sensor's response time. Such a parameter can be optimized in the model based on the gas sensor's target specifications.

In this analysis, the initial setup was the same as in the steady-state analysis. (A 2.5V bias was first applied to the microheater.) The time increment was 10 ms, and the end time was 5s. The plot in Figure 6 shows that our microheater takes ~0.35 s to reach a temperature of 400 °C and ~5 s to reach a steady-state temperature at ~960 °C. A bias of 1.4V leads to a steady-state temperature of ~400 °C, which also reached in 5 s.

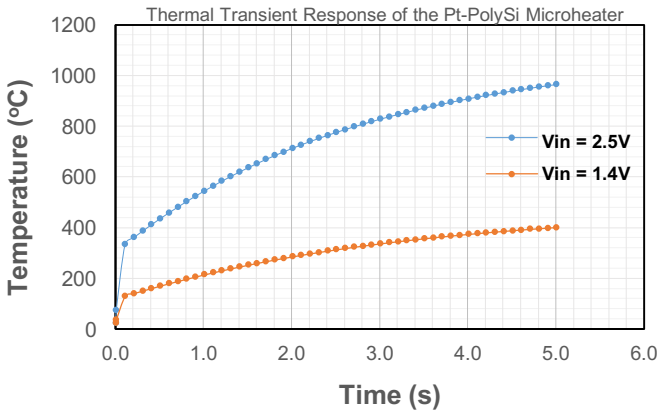

Figure 6. Microheater's simulated transient thermal response.

5. Conclusion

The purpose of this work was to understand the thermal transient response of a microheater, in addition to its steady-state behavior. Relatedly, we optimized the microheater's geometry for two purposes. One goal was to obtain a uniform steady-state temperature distribution. A second goal was to reach a 400 °C temperature within 0.5 seconds. Future work would be to add a gaseous environment around the model in order to simulate the chemical reaction of SnO_2 and target gases.

6. References

1. Ju, Y.S. and K.E. Goodson, *Process-dependent thermal transport properties of silicon-dioxide films deposited using low-pressure chemical vapor deposition.* Journal of Applied Physics, 1999. **85**(10): p. 7130-7134. 0021-8979.
2. Materials, A. *Tin Oxide (SnO_2) Stannic Oxide - Properties and Applications*. 8/6/2018]; Available from: https://www.azom.com/article.aspx?ArticleID=2358.
3. Materials, A. *Platinum (Pt) - Properties, Applications*. Available from: https://www.azom.com/article.aspx?ArticleID=9235.
4. Goodson, K.E., et al., *Annealing-temperature dependence of the thermal conductivity of LPCVD silicon-dioxide layers.* IEEE electron device letters, 1993. **14**(10): p. 490-492. 0741-3106.
5. Shi, L., et al. *Thermal conductivities of individual tin dioxide nanobelts*. 2004. American Society of Mechanical Engineers.
6. Materials, A. *Tin Dioxide (SnO_2) Semiconductors*. 8/6/2018]; Available from: https://www.azom.com/article.aspx?ArticleID=8456.

7. Takahashi, Y., *High-temperature heat-capacity measurement up to 1500K by the triple-cell DSC.* Pure and applied chemistry, 1997. **69**(11): p. 2263-2270. 1365-3075.

8. Materials, A. *Silica - Silicon Dioxide (SiO_2)*. [cited 2018 8/6/2018]; Available from: https://www.azom.com/properties.aspx?ArticleID=1114.

9. Isono, T., et al., *Highly conductive SnO_2 thin films for flat-panel displays.* Journal of the Society for Information Display, 2007. **15**(2): p. 161-166. 1071-0922.

10. Giancoli, D.C., *Physics: Principles with Applications*. 1995: Printice-Hall.

11. Mammana, A.P., et al. *Resistance behavior of thin SnO_2 films at high temperature*. in *LatinDisplay & IDRC 2012*. 2012. Sao Paulo.

12. Saberi, M.H., Y. Mortazavi, and A.A. Khodadadi, *Dual selective Pt/SnO_2 sensor to CO and propane in exhaust gases of gasoline engines using Pt/$LaFeO_3$ filter.* Sensors and Actuators B: Chemical, 2015. **206**: p. 617-623. 0925-4005.

13. Eranna, G., *Metal oxide nanostructures as gas sensing devices*. 2016: CRC Press.

14. El-Kareh, B., *Fundamentals of Semiconductor Processing Technology*. 1995, New York: Springer.

15. Madelung O., R.U., Schulz M, *Tin dioxide (SnO_2) optical properties, dielectric constants*. 1998, Springer-Verlag Berlin Heidelberg.

16. Lang, W., *Heat transport from a chip.* IEEE Transactions on Electron Devices, 1990. **37**(4): p. 958-963. 0018-9383.

17. Zhang, K.L., S.K. Chou, and S.S. Ang, *Fabrication, modeling and testing of a thin film Au/Ti microheater.* International Journal of Thermal Sciences, 2007. **46**(6): p. 580-588. 1290-0729.

7. Acknowledgment

This paper was made possible, in part, through travel support from the School of Graduate Studies at Case Western Reserve University.